ISSN 1560-0904, Polymer Science, Series B, 2022, Vol. 64, No. 5, pp. 657–669. © Pleiades Publishing, Ltd., 2022.
ISSN 1560-0904, Polymer Science, Series B, 2022. © Pleiades Publishing, Ltd., 2022.
Russian Text © The Author(s), 2022, published in Vysokomolekulyarnye Soedineniya, Seriya B, 2022, Vol. 64, No. 5, pp. 352–364.

DESTRUCTION OF POLYMERS

Features of Thermo-Oxidative Degradation and Pyrolysis of Nanocomposites Based on Porous Polyethylene and Silica

E. O. Fomin[a,*], E. S. Trofimchuk[a], M. A. Moskvina[a], and N. I. Nikonorova[a]

[a] *Department of Chemistry, Moscow State University, Moscow, 119991 Russia*

**e-mail: evgeniy_fomin_2000@bk.ru*

Received May 18, 2022; revised August 16, 2022; accepted August 30, 2022

Abstract—Effect of the structural mechanical modification via the crazing mechanism and composition of films based on HDPE nanocomposites and highly dispersed silica particles on the thermo-oxidative degradation and pyrolysis is studied. The incorporation of highly dispersed silica particles into the polymer matrix causes a reduction in the onset temperature of the intense weight loss of the composites by about 30°C and an increase in the temperature interval by 100°C under conditions of thermo-oxidative degradation. It is shown that in pyrolytic decomposition the HDPE–SiO_2 composite also starts to lose weight at lower temperatures (smaller by 50°C). Using various kinetic approaches to process the TGA curves the activation energy for each stage of thermal oxidation and pyrolysis is determined for structurally different HDPE-based samples. In the case of thermo-oxidative degradation, dependence of the activation energy on conversion is shown to be complex, thereby reflecting the multistage nature of the process. In pyrolysis, the activation energy is almost constant at all stages of the process. For various models of the processes, the activation energy is calculated by the Coats–Redfern method and the most probable mechanisms of thermal degradation and pyrolysis of the samples are proposed.

DOI: 10.1134/S1560090422700403

INTRODUCTION

The thermal stability of polymers and their composites is the decisive characteristic when choosing their application areas [1, 2]. At present, the thermal degradation of plastics is considered one of the most important methods for their processing into valuable chemical products [3]. It is known that the pyrolysis of low- and high-density polyethylenes yields various fractions of gaseous and liquid hydrocarbons in a high yield depending on temperature and process conditions which can be used as chemical products for organic synthesis [4–6]. In addition, burning is one of the main utilization methods for hard-to-decompose polymer waste [7]. Therefore, the study of thermal stability and pyrolysis processes (process kinetics and thermodynamics) and the analysis of reaction products as a function of temperature, heating rate, and composite composition are very topical. Similar studies enable the targeted control over the processes of thermal oxidation and pyrolytic cleavage of polymer chains.

One of the approaches to solve such problems includes the use of polymer composite materials with a certain level of mutual dispersity of components. The introduction of inorganic nanoparticles into polymers makes it possible to vary their physicochemical properties (thermal stability, rigidity, electrical conductivity, etc.) [8, 9]. Silica SiO_2 is a much-used filler due to its environmental friendless and low cost. Silica is added to commercial large-tonnage polymers to improve their mechanical and barrier properties and increase thermal stability [10–13]. These materials can be used in the production of food packaging, flexible electronics, or pharmaceutical packaging [14, 15].

As was shown earlier [16, 17], the introduction of inorganic nanoparticles leads to a change in thermal stability of the polymer matrix in relation to the chemical nature and dispersity of the filler. For example, highly dispersed particles of variable valence metals (Cu, Fe, Ti) exhibit the highest catalytic activity in initiation of polyolefin degradation processes, activating hydroperoxide decomposition and facilitating decrease in the activation energy of the oxidation reaction from 115 to 70–75 kJ/mol [16]. In contrast, the incorporation of 0.5 wt % of inert silica and titania into poly(methyl methacrylate) increases the activation energy of thermal decomposition from 69 to 99 kJ/mol. This phenomenon is explained by the fact that, in the presence of an inorganic filler in a composite, the mobility of polymer chains slows down and the impact of free radicals on polymer main chains weakens [18]. A rise in the thermal stability of polypropyl-

ene in thermo-oxidative degradation processes in the presence of silica and titania was described in [19].

Polyethylene is a widespread plastic (it accounts for 30% of the global plastics market [20]). Owing to its attractive physical and mechanical properties, lost cost, and easy processing its application in various industries as films, fibers, and matrices for polymer composites is growing. The introduction of special fillers allows the application of polyethylene in the manufacture of materials with new functional properties [21]. Research of the thermal stability of variable composition nanocomposites based on mesoporous HDPE films and highly dispersed silica phase, which are obtained according to the crazing methodology, and determination of the activation energy of their pyrolysis and thermo-oxidative degradation using various integral and differential mathematical methods to analyze the TGA data are the purposes of this study, and the posed task seems to be topical.

EXPERIMENTAL

Porous polymer matrices and their nanocomposites were obtained from the commercial HDPE film (Dorkhimzavod, Russia) with $M_w = 2 \times 10^5$, thickness 75 μm, T_m = 130°C, and the degree of crystallinity 70%. The uniaxial stretching of initial HDPE films in the medium of *n*-heptane (analytical grade, Khimmed) to a strain of 400% was carried out at 20–25°C at a rate of 25%/min using manual clamps. After deformation, the films were fixed around the perimeter in special frames to prevent their low-temperature shrinkage. The porous structure of the samples was characterized by the effective bulk porosity, which was determined as the ratio of volume increment to the final volume of the sample after tension. The morphology of the pores formed was visualized by AFM [22].

To obtain HDPE–SiO_2 nanocomposites the filler phase was synthesized in situ directly in pores of the polymer matrix according to the sol-gel technology. To do this, a liquid organosilicon precursor, hyperbranched polyethoxysilane (HPEOS, synthesized at the Enikolopov Institute of Synthetic Polymeric Materials, Russian Academy of Sciences) with M_w = 3×10^4 (density 1.17 g/cm^3, viscosity 18.8 mPa s, effective diameter of molecules of 2–5 nm), or its solutions in isopropanol (reagent grade, Khimmed, 5–25 wt %) were used to impregnate the as-formed porous HDPE films for 3 h. The samples with the introduced precursor were placed in a desiccator over a 10% HCl aqueous solution for 24–48 h. The obtained composite films were washed with distilled water and dried at room temperature until a constant weight was achieved. The resulting porous and composite samples were annealed at 100°C for 1 h to remove the unbound water and stabilize geometric sizes.

The structure of the composites was studied by X-ray diffraction on a Rigaku SmartLab instrument (CuK_α-radiation, λ = 0.154 nm) equipped with a rotating copper anode. X-ray diffraction patterns were measured in the transmission mode using a Pilatus 100k Dectris detector. The exposure time was 1500 s. Lupolen was used as a calibration standard. The data were processed using Fit2D and ImageJ software.

Morphological measurements were performed by TEM on a Leo-912 AB Omega microscope (K. Zeiss, Germany). Ultrathin sections of the composites were preliminarily prepared by ultramicrotoming using a diamond knife at room temperature (Reichert-Jung ultramicrotome, Germany) and then placed onto copper grids coated with the collodion substrate film.

The pyrolysis and thermo-oxidative degradation of the samples were studied by TGA on a TG50 Mettler-Toledo instrument equipped with an M3 microbalance in a flow of gas (nitrogen or air, respectively) of 200 mL/min in the dynamic regime at a rate of 10, 20, and 30 K/min in the range from 35 to 700°C. For these studies, samples 6.5 mm in diameter were cut from the films and placed in one layer in a ceramic cup. Thermograms were processed using the MetlerTC11 software. For each sample type and heating rate, three curves were obtained which demonstrated a sufficiently good reproducibility: on the temperature scale error did not exceed ±5°C; on the weight loss scale, error was ±4%.

RESULTS AND DISCUSSION

Structural and Morphological Studies

The thermal stability of polymers in pyrolysis and thermo-oxidative degradation processes depends not only on the chemical nature of macromolecules but also on their structural parameters, such as degree of crystallinity, orientation of crystallites, porosity, etc. [23, 24]. This study is focused on the systematic structural and morphological measurements of porous and composite samples. The porous structure of the HDPE film was formed during the uniaxial stretching of the polymer in the medium of *n*-heptane. The uniaxial deformation of the polymer in physically active media was studied in detail in [25–27]. It was shown that this process develops according to the intercrystallite crazing mechanism and is accompanied by pore formation. The structure of the porous HDPE film stretched to a strain of 400% was visualized by AFM (Fig. 1). The morphology of this film represents a system of disjoined fibrills localized in intercrystallite regions between which anisotropic pores with dimen-

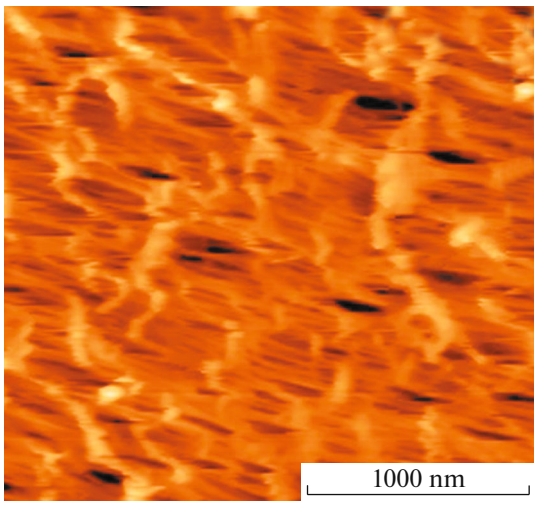

Fig. 1. AFM image of the HDPE porous film deformed to a strain of 400% according to the intercrystallite crazing mechanism.

sions of 20–30 nm (width) × 130 nm (length) elongated in the stretching direction are located. The value of the effective bulk porosity of similar films is about 40 vol %.

The deformation of polymers in physically active media is accompanied by development and formation of the specific fibrillar porous structure, and simultaneously the orientation of macromolecules proceeds. The orientation factor f_c was determined by the formula $f_c = (180° - \Delta\varphi_{1/2})/180°$, where $\Delta\varphi_{1/2}$ is the half-width of azimuthal intensity distribution of wide-angle X-ray scattering for the reflection of HDPE (110). It turned out that the initial HDPE film is weakly oriented: f_c is ~0.4. Stretching leads to a considerable gain in orientation, and at a strain of 400% the value of f_c grows to 0.95, thereby suggesting formation of the highly oriented structure.

Formation of the specific fibrillar porous structure in HDPE facilitates not only acceleration of the processes of oxygen diffusion inside the polymer, including thermal oxidation, but also the possible "encapsulation" of its certain amount inside the polymer matrix. Moreover, creation of the porous structure noticeably decreases heat conductivity of the polymer film [27]. Thus, when creating the porous structure in the polymer via orientational stretching two competing factors arise which can affect the degradation processes, namely, the amount of "encapsulated" oxygen is determined by the bulk porosity and it decreases with increasing orientational order. Development of a similar porous structure by the crazing mechanism can be regarded as an additional factor controlling the thermal oxidation and pyrolysis of polymer materials. A similar multidirectional impact of these parameters on the processes of the thermo-oxidative degradation of HDPE was observed in [28].

Nanocomposite materials were obtained by the synthesis of silica particles directly the pore volume of polymer matrices as described in [12, 29]. Since the synthesis of silica $SiO_2 \cdot nH_2O$ occurs only in crazes of the porous polymer matrix, its morphology can be varied by changing precursor concentration and nature. This is an effective approach to manufacturing filled nanocomposite materials with the controlled distribution of inorganic nanoparticles in the organic matrix. As is clear from the TEM microphotographs of thin sections (Fig. 2), the distribution of silica in the polymer bulk is fairly uniform.

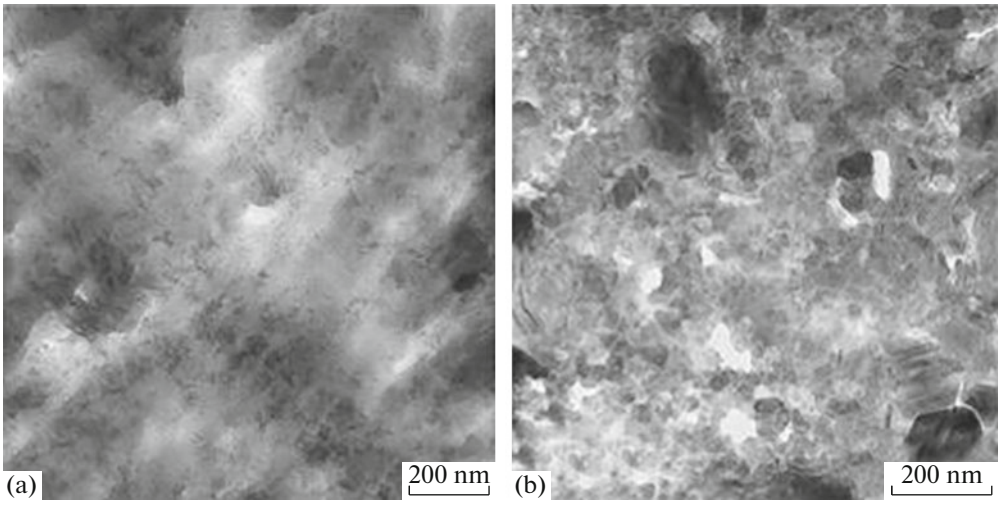

Fig. 2. TEM micrographs of ultrathin sections of HDPE-based composites containing (a) 10 and (b) 60 wt % SiO_2.

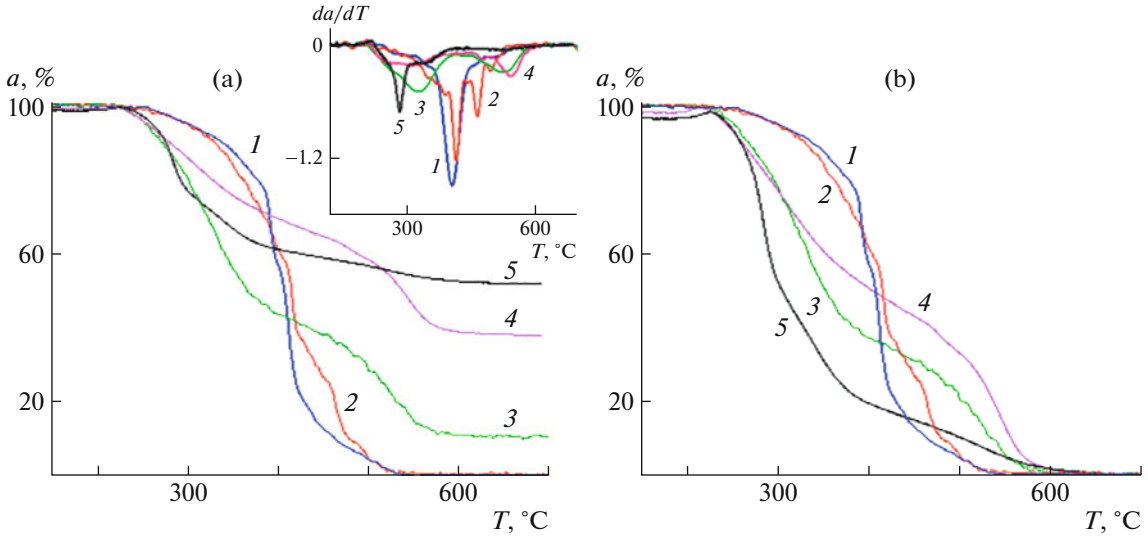

Fig. 3. Integral TGA curves (a) before and (b) after recalculation to the polymer content in the composite for (*1*) initial and (*2*) porous HDPE films and HDPE–SiO_2 composite containing (*3*) 10, (*4*) 40, and (*5*) 60 wt % SiO_2. The insert shows the differential TGA curves obtained in an air atmosphere at a heating rate of 10 K/min.

At the content of the second component on the order of 10 wt % fine discrete nanoparticles ~5 nm in size as well as larger aggregates with sizes of 20–30 nm are detected in the composite bulk. At a high content the continuous silica phase of the network-type composed of particles 15–25 nm in diameter is formed.

Thus, the introduction of silica apparently does not disturb the highly dispersed oriented structure of the polymer matrix but when filling pores can affect its gas permeability, thermal conductivity, and, hence, thermo-oxidative degradability.

Peculiarities of Thermo-Oxidative Degradation

At present, the processes of thermal degradation have been examined in a sufficient detail and the mechanisms underlying the decomposition of polyolefins have been elucidated [30–32]. The simplified mechanism of polyethylene oxidation by oxygen involves four stages [31, 33]. At the first stage of initiation oxygen induces the cleavage of macromolecules and peroxide radicals arise. Then peroxide oxidation of the sample corresponding to the stage of chain process propagation proceeds. At the third stage of chain branching, peroxides decompose and C–C bonds are cleaved more intensively to afford macroradicals and subsequent chain transfer. As a result, transverse bonds (crosslinks), including coke, are formed. At the final stage of chain termination, the reaction occurs by the mechanisms of thermo-oxidative degradation and thermal degradation of crosslinked structures. The thermal oxidation of polyolefins is described in more detail in Appendix 1. All these processes yield oligomeric and low molecular weight products that are removed from the polymer material; therefore, it weight decreases.

The kinetics of thermal degradation of PE (the activation energy, the position of temperature intervals of various stages) can be influenced by both the molecular structure of the polymer and the degree of orientation of macromolecules and SiO_2 nanoparticles incorporated into the sample matrix. Indeed, HDPE nanoporous matrices obtained by the crazing mechanism burn without dripping to yield coke [28]. This burning process is associated with both feasible chemical modification of the polymer during its deformation in the physically active medium and structural rearrangements of the polymer accompanied by orientation and pore formation. It was shown that creation of the porous structure according to the crazing mechanism shifts the onset temperature of the weight loss process to lower temperatures; an increase in orientation, to higher temperatures.

Figure 3a shows thermograms which were obtained under heating in an air atmosphere for various samples of HDPE (initial and porous) and its composites with the content of silica (in terms of SiO_2) in the range from 10 to 60 wt %. For the initial and porous HDPE films the TGA curves differ insignificantly (Fig. 3a, curves *1*, *2*). They have similar shapes and are characterized by close temperature intervals of the intense weight loss. Possibly, this can be attributed to the fact that porous films with a strain of 400% obtained herein possess a higher bulk porosity (almost by a factor of 2)

than those described in [28]. Since porosity and orientation affect position of the weight loss onset temperature in different directions, these two factors apparently level off each other.

Substantial differences are observed for the TGA curves of the composites (Fig. 3a, curves *3*–*5*): the curves assume a more complex, stepwise loss weight pattern. When their heating is completed a white solid always remains which was previously identified as SiO_2 [12] and the amount of which is proportional to the filler content in the sample. To gain a more clear understanding of the effect of filler content on the thermo-oxidative degradation of the HDPE matrix the experimental TGA curves were reconstructed taking into account the content of SiO_2 (Fig. 3b). It is seen that on average the rate of weight loss on any section of the curves for all composites is lower or does not exceed the rate of weight loss for the initial or porous film. It was shown that for the composites containing 10 and 40 wt % SiO_2 the curves are fairly close and have a similar pattern. The composite with the highest content of SiO_2 (60 wt %) loses weight much faster in the low-temperature range—up to 400°C its losses in terms of the polymer are on the order of 80%. This phenomenon is likely associated with a more reactive finely dispersed fibrillar structure of HDPE which preserves stability in the presence of a high concentration of the solid nanofiller. It is worth noting that regardless of the composition of the composites a section appears on the TGA curves approximately in the middle of the temperature interval of the intense weight loss (370–490°C) on which the rate of the process is decreased considerably. It can be assumed that this is related to the formation of oxygen inaccessible coke residue in porous SiO_2 which burns at higher temperatures. For the composite with the highest filler content this stage is the most distinct (Fig. 3b, curve *5*). This section is observed on the TGA curve of the porous HDPE film in the range of 430–460°C (Fig. 3b, curve *2*). This finding may also indicate that for the structurally modified samples the coking process is facilitated.

The mathematical processing of the thermograms was performed with the use of several kinetic methods described in Appendix 2. Temperature intervals for the stages of thermo-oxidative degradation were determined by the Coats–Redfern method [34, 35]. To this end, the dependence of $\ln(g(x)/T^2)$ on $1/T$ was plotted for each heating rate and linear sections were determined on these curves. The temperature intervals of thermo-oxidative degradation and the corresponding weight losses of the polymer are listed in Table 1. An increase in the rate of heating primarily leads to the shift of intervals to higher temperatures. It is seen that for the initial and deformed films the onset and end temperatures of the weight loss process are similar. For the initial HDPE there are four temperature intervals which are in good agreement with the stages of thermo-oxidative degradation described in [31, 33]. The most intense weight loss (on the order of 60%) is observed at the third stage—oxidative chain branching. For the porous film the temperature intervals of the first three stages are the same as those for the initial film. However, already at the second stage (oxidative chain propagation) a sufficiently intense weight loss is observed. The distinctive feature of the thermo-oxidative of the structurally modified film is that the fourth stage of the process (formation of crosslinked structures, char) is as if decomposed into two temperature intervals. It can be proposed that initially the intense char formation proceeds that hampers the access of oxygen; therefore, the rate of polymer weight loss decreases. At higher temperatures a more intense process related to burnout of the formed char residue begins.

Upon the introduction of silica into the polymer matrix the onset temperature of the weight loss decreases by 25–35°C and the whole process is completed by about 600°C. This provides evidence that for the composites the temperature interval of thermo-oxidative degradation widens by 100°C compared with the initial and porous HDPE films. An increase in the content of silica in the samples does not cause any marked change in the temperature intervals; however, the rate of weight loss at each stage changes. Note that the most considerable weight losses at the fourth stage (33%) are typical for the composite containing 40 wt % SiO_2 which may point to the maximum coking ability of this material. In further studies the effect of highly dispersed SiO_2 particles on the kinetic parameters of degradation processes were analyzed and determined using the composite containing 10 wt % silica as an example. The curves corrected for the filler content in the composite were used in calculations.

The activation energy of the thermal oxidation process was estimated by the Friedman differential method and Flynn–Wall–Ozawa (FWO) and Kissinger–Akahira–Sunose (KAS) integral methods [34, 35] described in Appendix 2. It is known that the application of integral isoconversional methods may lead to an error in determination of the activation energy compared with differential methods. However, differential methods are prone to considerable errors when dx/dT is small. Therefore, to obtain the most reliable information these methods should be combined. Herein dependence of the activation energy on conversion was constructed using the average value of the activation energy calculated by the three methods. The results are presented in Fig. 4. Furthermore, the activation energy ΔE_a of each stage was calculated as a difference between the local energy minimum and maximum (Table 2). In addition, the most probable mechanisms were determined for the each stage of degradation of the tested samples. For this purpose, the Coats–Redfern method was applied to calculate

Table 1. Temperature intervals for stages of the thermo-oxidative degradation of HDPE-based samples at a heating rate of 10 K/min

Sample	Content of SiO_2, wt %	Temperature interval, °C	Weight loss*, %
Initial HDPE	0	250–280	5
		285–370	15
		375–425	60
		430–530	20
Porous HDPE	0	250–300	6
		300–380	25
		390–420	30
		425–460	16
		465–530	23
Composite HDPE–SiO_2	10	215–275	12
		280–360	41
		370–480	23
		490–580	24
	40	215–265	12
		270–365	31
		370–490	24
		500–620	33
	60	225–290	40
		300–380	38
		385–490	12
		500–620	10

* The data are presented after correction for the residue weight upon heating to 700°C.

Table 2. The activation energy and mechanisms describing the stages of decomposition of HDPE-based samples

Stage	HDPE			Porous HDPE			HDPE–SiO_2		
	mechanism	E_a, kJ/mol	ΔE_a, kJ/mol	mechanism	E_a, kJ/mol	ΔE_a, kJ/mol	mechanism	E_a, kJ/mol	ΔE_a, kJ/mol
1	S3	60 ± 5	60	*	80 ± 15	80	D1	170 ± 5	170
2	D	190 ± 5	135	D	115 ± 5	35	*	115 ± 10	–
3	F3/S5	285 ± 5	95	F1	220 ± 5	95	*	130 ± 10	20
4	*	360 ± 25	180	F3	300	140	F2	165 ± 5	115
				D	70 ± 10	–			

the activation energy for standard functions $g(x)$ listed in the table of Appendix 2 and the data obtained were compared with the absolute values of the activation energy derived from the experimental data. Symbol (*) in Table 2 means that the mechanism cannot be described by one model, since none of the values of the activation energy coincides with that calculated for a certain mechanism. It appears that several models are realized in this case, and the activation energy is calculated as a sum of activation energies for these mechanisms.

As is seen from Fig. 4, for the initial and porous samples there are two maxima; for the composite,

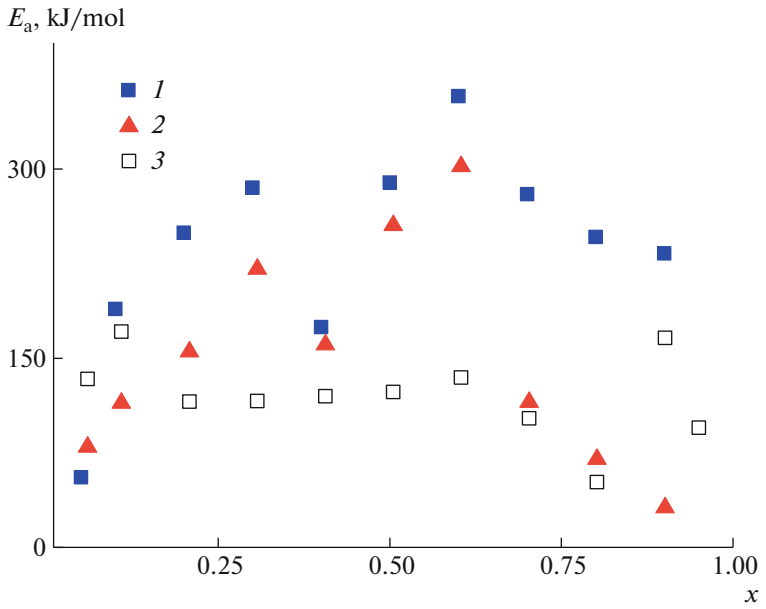

Fig. 4. Conversion dependence of the activation energy for (*1*) initial and (*2*) porous HDPE films and (*3*) HDPE–SiO_2 composite containing 10 wt % SiO_2.

three maxima. The positions of the maxima for the initial and porous films on the conversion axis coincide (at $x = 0.3$ and 0.6). However, for the initial film the absolute values of the activation energy are higher. For the composite film the maxima are detected at $x =$ 0.1, 0.6, and 0.9. Comparing the results shown in Table 2 for the initial film makes it possible to assign the observed maxima to the activation energies of the third and fourth degradation stages (Fig. 4, curve *1*) which corresponds to chain process branching and kinetic chain termination. Note that the first two stages of chain initiation and propagation are characterized by relatively low absolute values of the activation energy and small weight losses—conversion is below 0.2. This is presumably due to the fact that at the third and fourth stages the processes cannot be described by any one mechanism but only by their combination, each of which contributes to the absolute value of the activation energy. It should be mentioned that the values of ΔE_a determined for each stage of degradation of the initial HDPE film summarized in Table 2 are well consistent with the data reported in [36].

For porous HDPE the values of the activation energy at all conversions are lower than that for the initial film. Probably, this can be explained by the fact that during melting of the porous film air contained in pores is encapsulated in the sample bulk because of a high viscosity of the polymer melt (~10^5 P). As a result, the number of accessible "active" centers, where oxidation of the polymer and generation of peroxide radicals can take place, grows. In this case, the stages of oxidative chain initiation and propagation proceed faster and more intense, for example, the weight loss for the porous sample at the second stage is 10% higher than that for the initial HDPE. This is also indicated by a very low value of $\Delta E_a = 35$ kJ/mol for the second stage while for third and fourth stages with the initial sample the values of ΔE_a are similar (Table 2). It is of importance that for the structurally modified porous sample the fourth stage of oxidative chain termination accompanied by char formation and its subsequent burnout is decomposed into two temperature intervals, at each of which the process characterized by its own activation energy proceeds.

For the HDPE–SiO_2 composite the highest activation energy 170 kJ/mol corresponds to the stage of oxidative chain initiation. This may be related to a reduced gas permeability of the filled material, in which the formed silica phase fills pores and thus may hamper penetration of air inside the sample. For this stage the process of diffusion turns out to be limiting. The lowest activation energies correspond to the second and third stages, and the Coats–Redfern method does not allow their separation. This may indicate that degradation of the composite accompanied by weight loss is facilitated in the presence of the nanosized SiO_2 phase with a highly developed surface. On the contrary, silica apparently hinders the burnout of char formed in its pores which may lead to a certain rise in the activation energy for the fourth stage and thus decelerate the process of weight loss.

Thus, our results demonstrate that development of the porous oriented structure according to the crazing mechanism and introduction of SiO_2 nanosized parti-

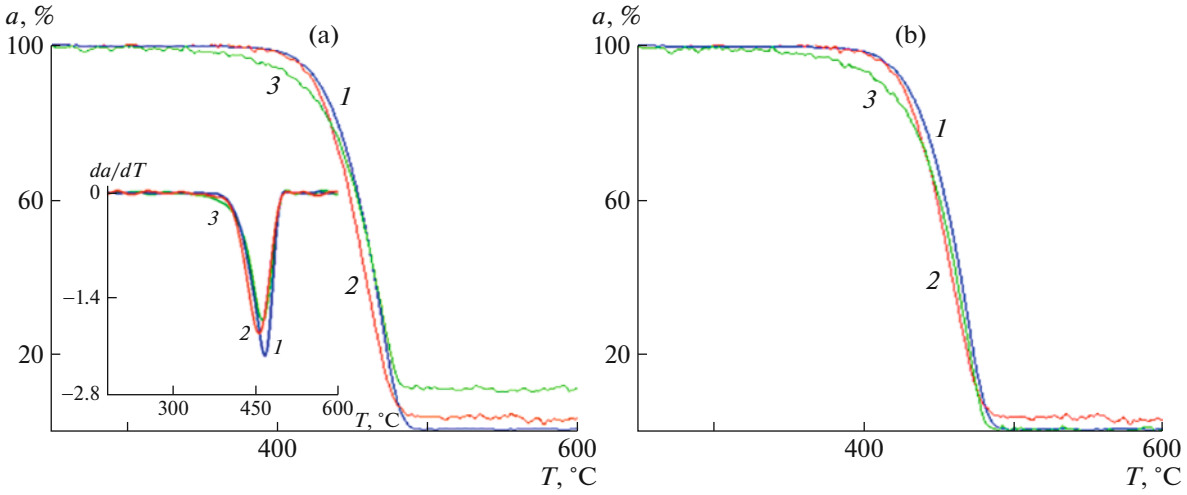

Fig. 5. Integral TGA curves (a) before and (b) after recalculation to the polymer content in the composite for (*1*) initial and (*2*) porous HDPE films and (*3*) HDPE–SiO_2 composite containing 10 wt % SiO_2. The insert shows differential TGA curves obtained in a nitrogen atmosphere at a heating rate of 10 K/min.

cles contribute to reduction in the activation energy of the thermal oxidation of HDPE and make it possible to redistribute the contribution of each stage to the total process of polymer degradation, and this should reflect on the composition of final products.

Effect of Structural and Mechanical Modification on the Processes of Pyrolytic Decomposition of HDPE

The kinetic study of pyrolytic decomposition and the analysis of reaction products and degradation mechanism are an important tool for polymer recycling processes on the industrial scale [35]. Possibilities to control the yield of pyrolysis products at both qualitative and quantitative level open new prospects for plastics recycling. The systematic kinetic analysis of the pyrolysis process is crucial for revealing degradation mechanisms. This study addresses the pyrolysis of HDPE which was modified by creating a specific oriented fibrillar porous structure according to the crazing mechanism.

Figure 5a shows the TGA curves obtained during heating of the initial and structurally modified films of HDPE and HDPE–SiO_2 composite in a nitrogen atmosphere. Under these conditions the thermolysis of polymer chains takes place. It should be noted that construction of the TGA curve for the composite with allowance for the filler content does not change it considerably (Fig. 3b, curve *3*) compared with thermo-oxidative degradation. It is seen that pyrolytic decomposition of the polymer starts at a temperature 100–150°C higher than thermal oxidation. Note that the composite loses weight about 50°C earlier than the unfilled samples. The reason behind this phenomenon is still unclear. This is probably associated with the heterogeneous structure of the composite sample and unequal heat conductivities and heating rates of its different parts. For all samples pyrolysis is completed at about 500°C. For the porous HDPE film 4 wt % of the solid residue remains after pyrolysis. This result correlates well with the data reported in [28]. The authors of [28] first showed that the burning of porous HDPE films is accompanied by char formation. The differential TGA curves (insert in Fig. 5a) measured for all types of the samples exhibit only a single peak. It is generally accepted [34] that this fact may testify that formally the pyrolysis process proceeds in one step, although noting suggests mechanisms of this process.

Table 3. Temperature interval of pyrolysis and temperature of the maximum weight loss at a heating rate of 10 K/min for HDPE-based samples

Sample	Temperature interval, °C	T_{peak}, °C
HDPE	395–490	465
Porous HDPE	385–485	455
Composite HDPE–SiO_2 (10 wt %)	340–485	460

Table 3 lists temperature intervals of the pyrolytic decomposition of the tested samples and temperatures of the maximum weight loss which are found to be similar. With an increase in the rate of heating, as in the case of thermo-oxidative degradation, the TGA curves shift to higher temperatures.

The activation energy was estimated by the Friedman, FWO, and KAS methods. For the composite calculation was performed using curves corrected for the content of SiO_2. Figure 6 displays the conversion dependences of the activation energy. As is seen for the initial HDPE film, the activation energy is almost

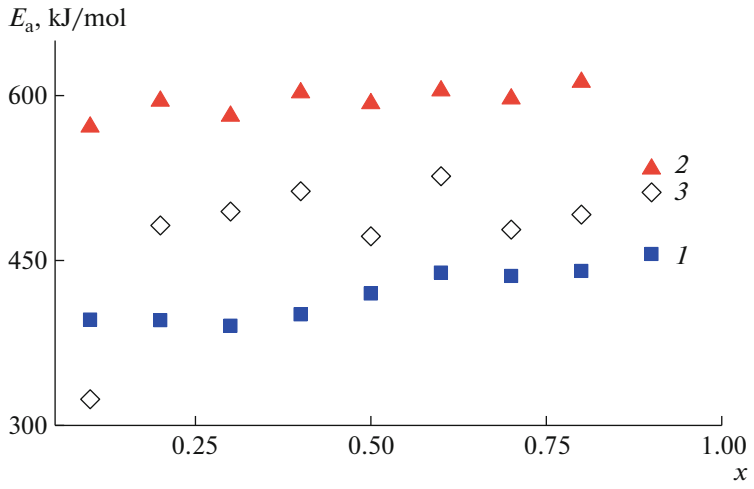

Fig. 6. Conversion dependence of the activation energy for (*1*) initial and (*2*) porous HDPE films and (*3*) HDPE–SiO_2 composite containing 10 wt % SiO_2.

constant in the conversion range from 0.1 to 0.9 and its absolute value is on the order of 400–450 kJ/mol. Slight deviations are observed for initial and final stages of the reaction which may be associated with the error that manifests itself in the Friedman method at small weight changes with temperature. For the porous HDPE film the total activation energy of the pyrolysis process grows by almost 1.5 times to 600 kJ/mol. This may be due to the fact that the mentioned methods make it possible to calculate the absolute value of the activation energy which is the sum of activation energies of simultaneous processes proceeding via different mechanisms. In this case, it is naturally to assume that presence of the encapsulated oxygen in the porous matrix can be responsible for appearance of the alternative degradation mechanisms under conditions of pyrolytic heating. The activation energies typical for the pyrolysis of the HDPE–SiO_2 nanocomposite are between the E_a values for the initial and porous films and have small local maxima equal to 515 and 525 kJ/mol at conversions $x = 0.4$ and 0.6, respectively.

To determine the most probable mechanisms of pyrolysis by the Coats–Redfern method the activation energies were calculated for all functions $g(x)$ listed in the table of Appendix 2 for cases of 10 K/min heating rates. The results are presented in Table 4.

When comparing the activation energies for the pyrolysis of HDPE (Fig. 6) with those calculated for different reaction mechanisms it can be supposed that diffusion mechanisms D are the most probable (limiting, with the highest activation energy) in this case. For the porous sample and composite this comparison is impossible. This may attest to a more intricate mechanism of pyrolysis in these systems which cannot be described by one model. This is apparently associated with the simultaneous occurrence of several pro-

Table 4. The activation energy and mechanisms describing the stages of decomposition of HDPE-based samples calculated by the Coats–Redfern method

HDPE		Porous HDPE		HDPE–SiO_2	
mechanism	E_a, kJ/mol	mechanism	E_a, kJ/mol	mechanism	E_a, kJ/mol
R1	213	R1	215	R1	130
R2	229	R2	236	R2	157
R3	235	R3	243	R3	167
D1	437	D1	442	D1	272
D2	458	D2	468	D2	306
D3	466	D3	478	D3	313
F1	248	F1	259	F1	187

cesses. In the presence of highly dispersed SiO_2 particles with a fairly high specific surface, all the examined possible model mechanisms of pyrolysis (Table 4) are implemented more easily, that is, operate with much lower activation energies (on average by 100 kJ/mol). The observed effects are important from the point of view of processing HDPE-based plastics by pyrolytic decomposition.

CONCLUSIONS

Study of the effect of the specific oriented fibrillar porous structure of HDPE films created by the crazing mechanism and highly dispersed silica particles on the processes of the thermal oxidation and decomposition of HDPE demonstrated that formation of the porous oriented structure exerts a slight effect on the thermal and thermo-oxidative stability of the polymer. The introduction of SiO_2 into the polymer matrix leads to a considerable reduction in the onset temperature of thermo-oxidative degradation and causes a marked increase (by 100°C) in the weight loss temperature interval.

The conversion dependence of the activation energy for thermo-oxidative degradation is found to be complex and can be represented by four stages. For the HDPE–SiO_2 composite at initial stages diffusion processes start to play the limiting role. Formally, pyrolytic decomposition is described as a one-step process for which the values of the activation energy for all tested samples are almost independent of conversion. The introduction of highly dispersed SiO_2 particles promotes a marked reduction in the weight loss onset temperature (by 50°C) under conditions of pyrolytic decomposition and a sharp decrease in the activation energy for all considered model mechanisms of this process within the framework of the Coats–Redfern method. However, for the porous films and composites the absolute values of E_a determined by the Friedman, FWO, and KAS methods are much higher than those calculated by the Coats–Redfern method which suggests the intricate mechanism of pyrolysis for the structurally modified samples.

Thus, the structural mechanical modification of the polymer via the crazing mechanism, which is accompanied by development of the fibrillar porous structure, and synthesis in the pores of highly dispersed phase of SiO_2 open additional possibilities to govern the processes of thermal oxidation and pyrolysis of plastics and their nanocomposites in order to attain their more effective utilization. At the same time, the kinetic study of the thermal decomposition of polymers is necessary for their feasible recycling.

APPENDIX 1

Peculiarities of the Thermo-Oxidative Degradation of Polyethylene

At the first stage oxygen-induced cleavage of polymer chains and generation of peroxide radicals take place, with the chain mechanism being initiated primarily in amorphous regions of the polymer and its rate depending on diffusion into the polymer bulk:

$$\text{(I)} \quad RH + O_2 \rightarrow R^{\bullet} + HO_2^{\bullet},$$

$$2RH + O_2 \rightarrow 2R + H_2O_2,$$

where RH is the monomer unit ~CH_2–CH_2~.

Then peroxide oxidation of the sample emerges which corresponds to the stage of chain propagation. It also proceeds without substantial degradation of the polymer and basically occurs in amorphous regions in the surface layer:

$$\text{(II)} \quad R^{\bullet} + O_2 \rightarrow RO_2^{\bullet},$$

$$RO_2^{\bullet} + RH \rightarrow ROH + RO^{\bullet},$$

$$RO_2^{\bullet} + RH \rightarrow ROOH + R^{\bullet},$$

$$RO_2^{\bullet} \rightarrow RO + HO^{\bullet},$$

$$RH + HO^{\bullet} \rightarrow R^{\bullet} + H_2O.$$

Ketones and alcohols are the key products at these stages. For polyethylene depolymerization is unlikely; however, under anaerobic conditions vinylene groups can be formed as a result of disproportionation. The weight loss at these stages is insignificant and is mostly related to the removal of low molecular weight products and the decomposition of hydroperoxides which are initially present in the material and are formed during the process.

At the third stage of chain branching the decomposition of peroxides, the main process, occurs as well as the decomposition of the polymer via the cleavage of bond C–C accompanied by the generation of macroradicals and subsequent chain transfer leading to transverse crosslinking of the polymer and formation of the system of branched bonds:

$$\text{(III)} \quad 2ROOH \rightarrow RO^{\bullet} + R^{\bullet} + H_2O,$$

$$ROOH \rightarrow RO^{\bullet} + {}^{\bullet}OH,$$

$$RCHO + O_2 \rightarrow R^{\bullet} + CO + HO_2^{\bullet}.$$

A low concentration of oxygen inside the polymer matrix, and, hence, the presence of a small amount of terminal peroxide groups increasing the rate of recombination also leads to the transverse crosslinking of the polymer.

At the stage of chain termination reactions IV proceed both via thermo-oxidative (1.1) and thermal degradation (1.2). The activation energy at this stage is maximum and amounts to 190–210 kJ/mol, which is comparable with the energy of chain termination in anaerobic thermal decomposition.

$$\text{(IV)} \quad R^{\bullet} + RO_2^{\bullet} \rightarrow ROOR \tag{1.1}$$

$$2RO_2^{\bullet} \rightarrow ROOR + O_2$$

$$2RO_2^{\bullet} \rightarrow ROOOOR \rightarrow RCHO + ROH + O_2$$

$$R^{\bullet} + R^{\bullet} \rightarrow R\text{–}R \tag{1.2}$$

$$R^{\bullet} + R^{\bullet} \rightarrow \sim CH{=}CH_2 + CH_3\text{–}CH_2\sim$$

All these processes result in formation of oligomeric and low molecular weight products which are removed from the material. The shift of the thermal effect to higher temperatures relative to the weight loss maximum is caused by coke formation on the surface of the sample during its thermal degradation.

APPENDIX 2

Methods for Describing Kinetics of the Thermal Degradation of Polymers

When describing kinetics of the thermal degradation of polymers the rate of decomposition of a polymer is usually assumed to be proportional to the concentration of the reacted material:

$$\frac{dx}{dt} = \beta\frac{dx}{dT} = K(T)f(x), \tag{2.1}$$

where x is the reaction conversion and β is the rate of heating. The rate constant is determined by the Arrhenius equation:

$$K(T) = A\exp\left(\frac{-E_a}{RT}\right), \tag{2.2}$$

where E_a is the activation energy and A is the preexponential factor. Then substituting equality (2.2) into Eq. (2.1) we get

$$\beta\frac{dx}{dT} = A\exp\left(\frac{-E_a}{RT}\right)f(x). \tag{2.3}$$

The Friedman method. If we take the logarithm of expression (2.3), then the activation energy can be easily obtained in a wide conversion range by constructing graph of $\ln\left(\beta\frac{dx}{dT}\right)$ against $1/T$ at constant x:

$$\ln\left(\beta\frac{dx}{dT}\right) = \ln. \tag{2.4}$$

This method makes it possible to found out how the reaction proceeds: rapidly (autocatalysis) or slowly (diffusion limited). Using the Friedman approach the stage nature of the process can also be determined.

The Kissinger–Akahira–Sunose (KAS) method. Equality (2.3) can be transformed into the following form:

$$\frac{dx}{f(x)} = \frac{A}{\beta}\exp\left(\frac{-E_a}{RT}\right)dT. \tag{2.5}$$

After integration of this expression under the condition that at $x = 0$ and $T = T_0$ we arrive at

$$g(x) = \int_{T_0}^{T}\frac{A}{\beta}\exp\left(\frac{-E_a}{RT}\right)dT = \frac{AE_a}{\beta R}p\left(\frac{E_a}{RT}\right). \tag{2.6}$$

Equation (2.6) can be integrated only under the assumption that A, E_a, $f(x)$ are independent of x. The KAS method is based on the Coats–Redfern approximation according to which

$$p\left(\frac{E_a}{RT}\right) \cong \frac{e^{-\left(\frac{E_a}{RT}\right)}}{\left(\frac{E_a}{RT}\right)^2}. \tag{2.7}$$

Taking the logarithm of expression (2.6) and substituting it into equality (2.7) we obtain

$$\ln\left(\frac{\beta}{T^2}\right) = \ln\left(\frac{AR}{E_a g(x)}\right) - \frac{E_a}{RT}. \tag{2.8}$$

Then plotting the graph of $\ln\left(\frac{\beta}{T^2}\right)$ against $1/T$ at $x = \text{const}$ we can calculate the activation energy from slope of the straight line.

The Flynn–Wall–Ozawa (FWO) method. This method is very similar to the KAS approach except that here the Doyle approximation is used

$$\ln\left(p\frac{E_a}{RT}\right) \cong -5.331 - 1.052\frac{E_a}{RT}. \tag{2.9}$$

Then equality (2.8) is transformed into the form

$$\ln(\beta) = \ln\left(\frac{AE_a}{Rg(x)}\right) - 5.331 - 1.052\frac{E_a}{RT}. \tag{2.10}$$

The main advantage of the FWO method is that the apparent values of the activation energy can be determined without knowing specific functions $f(x)$ and $g(x)$.

The Coats–Redfern method. This method uses the asymptotic approximation that $2RT/E_a \ll 1$, and then equality (2.6) can be transformed into the form

$$\ln\frac{g(x)}{T^2} = \ln\frac{AR}{\beta E_a} - \frac{E_a}{RT}. \tag{2.11}$$

It is known that the application of integral isoconversional methods (FWO, Coats–Redfern) may lead to the overestimated activation energy compared with differential methods. However, the differential methods are prone to significant errors when dx/dT is small. Moreover, these methods do not provide infor-

mation about the mechanism of reaction. To obtain reliable information these methods should be combined.

Algebraic expressions for functions of the most common reaction mechanisms

Mechanism	$f(x)$	$g(x)=\int\frac{1}{f(x)}dx$
R1 is the zero-order reaction	1	x
R2 is the 2D interface reaction	$2(1-x)^{1/2}$	$1-(1-x)^{1/2}$
R3 is the 3D interface reaction	$3(1-x)^{2/3}$	$1-(1-x)^{1/3}$
D1 is diffusion	$\frac{1}{2x}$	x^2
D2 is 2D diffusion	$\frac{-1}{2\ln(1-x)}$	$(1-x)\ln(1-x)+x$
D3 is 3D diffusion	$\frac{3}{2((1-x)^{-1/3}-1)}$	$\left(1-\frac{2}{3}x\right)-(1-x)^{2/3}$
S1 is the power law	$\frac{1}{4x^{\frac{1}{4}}}$	$x^{\frac{1}{4}}$
S2	$\frac{1}{3x^{\frac{1}{3}}}$	$x^{\frac{1}{3}}$
S3	$\frac{1}{2x^{\frac{1}{2}}}$	$x^{\frac{1}{2}}$
S4	$\frac{3}{2}x^{\frac{2}{3}}$	$x^{\frac{2}{3}}$
S5	$\frac{4}{3}x^{\frac{3}{4}}$	$x^{\frac{3}{4}}$
F1 is the first-order reaction	$1-x$	$-\ln(1-x)$
F2 is the second-order reaction	$(1-x)^2$	$\frac{1}{1-x}$
F3 is the third-order reaction	$(1-x)^3$	$\frac{1}{(1-x)^2}$

ACKNOWLEDGMENTS

We are grateful to A.M. Muzafarov for providing us with precursor hyperbranched polyethoxysiloxane, A.O. Dudnik for her help in AFM structural studies of the porous HDPE film, and A.V. Bakirov for his help in X-ray diffraction measurements.

FUNDING

This work was supported by the Russian Science Foundation (project no. 20-13-00178).

CONFLICT OF INTEREST

The authors declare that they have no conflicts of interest.

REFERENCES

1. R. Sudip and P. C. Ralph, *Handbook of Environmental Degradation of Material*, 3rd ed., Ed. by M. Kutz (William Andrew Publ., Norwich, 2018)
2. J. Koo, *Fundamentals, Properties, and Applications of Polymer Nanocomposites* (Cambridge University Press, Cambridge, 2016).
3. M. S. Abbas-Abadi, J. Therm. Anal. Calorim. **143** (300), 2867 (2021).
4. S. Kumar and R. K. Singh, J. Pet. Eng. **2013**, 1 (2013).
5. L. S. Diaz-Silvarrey, K. Zhang, and A. N. Phan, Green Chem. **20** (8), 1813 (2018).
6. D. Zhao, X. Wang, J. B. Miller, and G. W. Huber, Chem. Sus. Chem. **13** (7), 1764 (2020).
7. N. Evode, S. A. Qamar, M. Bilal, D. Barceló and H. M. N. Iqbal, Case Stud. Chem. Environ. Eng. **4**, 8 (2021).
8. Sh. R. Yashas, B. Shahmoradi, K. Wantala, and H. P. Shivaraju, Polymer **233**, 1 (2021).
9. M. S. A. Darwish, M. H. Mostafa, and L. M. Al-Harbi, J. Mol. Sci. **23** (3), 32 (2022).
10. H. Zou, S. Wu, and J. Shen, Chem. Rev. **108** (9), 3893 (2008).
11. V. Mittal, Materials **2** (3), 992 (2009).
12. N. I. Nikonorova, E. S. Trofimchuk, I. B. Meshkov, A. L. Volynskiia, N. F. Bakeev, and A. M. Muzafarov, Nanotechnol. Russ. **10** (11-12) 888 (2015).
13. D. W. Lee and B. R. Yoo, J. Ind. Eng. Chem. **38**, 1 (2016).
14. M. Zhang, G. M. Biesold, W. Choi, J. Yu, Y. Deng, C. Silvestre, and Zh. Lin, Mater. Today (2022), in press.
15. Q. Guo and X. Zhang, Compos. B. Eng. **227**, 1 (2021).
16. M. T. Bryk, *Destruction of Filled Polymers* (Khimiya, Moscow, 1989) [in Russian].
17. K. Król-Morkisz and K. Pielichowska, *Polymer Composites with Functionalized Nanoparticles* (Elsevier, Amsterdam, 2019), p. 405.
18. H. Wang, P. Xu, W. Zhong, L. Shen, and Q. Du, Polym. Degrad. Stab. **87** (2), 319 (2005).
19. E. S. Trofimchuk, V. V. Polyanskaya, M. A. Moskvina, T. E. Grokhovskaya, N. I. Nikonorova, A. L. Strembitskaya, A. L. Volynskii, and N. F. Bakeev, Polym. Sci., Ser. A **57** (1), 13 (2015).
20. C. Wang, Y. Liu, W. Chen, B. Zhu, S. Qu, and M. Xu, J. Ind. Ecology **25** (5), 1300 (2021).
21. P. M. Visakh and M. J. M. Morlanes, *Polyethylene Based Blends, Composites, and Nanocomposites* (Wiley Scrivener Publ. LLC, 2015).
22. A. O. Roenko, E. S. Trofimchuk, A. V. Efimov, G. A. Armeev, N. I. Nikonorova, A. Yu. Nikolaev, and A. L. Volynskii, Polym. Sci., Ser. A **62** (5), 471 (2021).
23. L. Shibryaeva, A. Popov, and G. Zaikov, *Thermal Oxidation of Polymer Blends: The Role of Structure* (CRC Press, London, 2006).

24. P. Gijsman, e-Polymers **8** (1), 65 (2008).
25. A. O. Dudnik, E. S. Trofimchuk, A. V. Efimov, N. I. Nikonorova, E. G. Rukhlya, L. N. Nikitin, I. V. Yaminsky, and A. L. Volynskii, Macromolecules **51** (3), 1129 (2018).
26. O. V. Arzhakova, A. Yu. Kopnov, A. I. Nazarov, A. A. Dolgova, and A. L. Volynskii, Polymer **186**, 1 (2020).
27. O. V. Arzhakova, A. I. Nazarov, A. R. Solovei, A. A. Dolgova, A. Y. Kopnov, D. K. Chaplygin, P. M. Tyubaeva, and A. Y. Yarysheva, Membranes **11** (11), 834 (2021).
28. E. S. Trofimchuk, M. Yu. Yablokova, N. I. Nikonorova, A. V. Antonov, A. L. Volynskii, and N. F. Bakeev, Polym. Sci., Ser. B **43** (7), 190 (2001).
29. E. S. Trofimchuk, I. B. Meshkov, M. N. Kandlina, N. I. Nikonorova, A. M. Muzafarov, I. A. Malyshkina, M. A. Moskvina, F. I. Grabovenko, and A. L. Volynskii, Macromol. Mater. Eng. **304** (11), Art. 1900430 (2019).
30. L. Costa and P. Bracco, *Mechanisms of Crosslinking, Oxidative Degradation and Stabilization of UHMWPE* (Academic Press: Burlington, 2009), Chap. 21.
31. M. Gardette, A. Perthue, J.-L. Gardette, T. Janecska, E. Földes, B. Pukánszky, and S. Therias, Polym. Degrad. Stab. **98** (11), 2383 (2013).
32. L. Shibryaeva, *Polypropylene*, Ed. by F. Dogan (Rijeka, Croatia, 2012), p. 63.
33. Y. Bolbukh, P. Kuzema, V. Tertykh, and I. Laguta, J. Therm. Anal. Calorim. **94** (3), 727 (2008).
34. A. Aboulkas, K. El Harfi, and A. El Bouadili, Energy Convers. Manag. **51** (7), 1363 (2010).
35. V. Mortezaeikia, O. Tavakoli, and M. S. Khodaparasti, J. Anal. Appl. Pyrolysis. **160**, 105340 (2021).
36. Y. Bolbukh, P. Kuzema, V. Tertykh, and I. Laguta, J. Therm. Anal. Calorim. **94** (3), 727 (2008).

Translated by T. Soboleva